

Complex Thermal Expansion Properties in a Molecular Honeycomb Lattice

Jonathan J. Loughrey^{a,b}, Tim P. Comyn^c, David C. Apperley^d,
Marc A. Little^{a,e} and Malcolm A. Halcrow^{*a}

^a*School of Chemistry, University of Leeds, Woodhouse Lane, Leeds, UK LS2 9JT.*

E-mail: m.a.halcrow@leeds.ac.uk

^b*Current address: Department of Chemistry and Biochemistry, University of Arizona,
P.O. Box 210041, 1306 East University Blvd., Tucson, AZ 85721-0041, USA*

^c*Institute for Materials Research, School of Process, Environmental and Materials Engineering,
University of Leeds, Clarendon Road, Leeds, UK LS2 9JT.*

^d*EPSRC Solid State NMR Service, Department of Chemistry, University of Durham, South Road,
Durham, UK DH1 3LE.*

^e*Current address: Department of Chemistry, University of Liverpool, Crown Street, Liverpool,
UK L69 7ZD.*

Electronic Supplementary Information

Experimental procedures and characterisation data.

Table S1 Experimental data for the single crystal structure determinations of **1**.

Figure S1 Contents of the asymmetric unit of **1** at 300 K and 110 K.

Table S2 Selected interatomic distances and angles in the crystal structures of **1**.

Table S3 Hydrogen bond parameters for the crystal structures in this work.

Table S4 Variable temperature unit cell parameters for **1** from single crystal and powder diffraction data.

Figure S2 An alternative set of single crystal unit cell data from **1**, measured using a different crystal.

Figure S3 Observed and simulated X-ray powder diffraction data from the different phases of **1**.

Figure S4 Changes to the X-ray powder diffraction pattern of **1** during *in situ* dehydration.

Figure S5 Thermogravimetric analyses (TGAs) of **1** and **2**.

Figure S6 Solid state ¹¹B NMR spectra of **1**, at 298, 238 and 168 K.

Figure S7 Solid state ¹⁹F NMR spectra of **1**, at 298, 238 and 168 K.

Figure S8 Variable temperature solid state ¹¹B NMR linewidths.

References

Synthetic Procedures and Characterisation Data for the Compounds in this Work.

3{5}-(Pyrazinyl)-1*H*-pyrazole (*L*) was prepared by the literature procedure,^[1] while all other reagents were purchased commercially and used as supplied. The complex [FeL₃][BF₄]₂·*x*H₂O (**1**) was prepared by mixing aqueous solutions of *L* (0.25 g, 1.7 mmol) and Fe[BF₄]₂·6H₂O salt (0.19 g, 0.6 mmol). Slow evaporation of the resultant deep red solution to dryness afforded clusters of brown needle-shaped crystals that were collected, dried and analysed without further purification. Found C, 35.2; H, 3.10; N, 23.2 %. Calcd. for C₂₁H₁₈B₂F₈FeN₁₂·3H₂O C, 35.0; H, 3.35; N, 23.3 %.

Elemental microanalyses were performed by the University of Leeds School of Chemistry microanalytical service. Thermogravimetric analyses employed a TA Instruments TGA 2050 analyser. X-ray powder diffraction was collected using a PANalytical X'Pert MPD diffractometer (Cu *K*_{α1+2}), with an *in situ* liquid N₂ cold stage (Anton Paar TTK450). Data were collected between 2θ = 5 and 50°, with a step size of 0.033°; the total time per scan was 20 mins. Rietveld refinements were prepared using PANalytical X'Pert *Highscore Plus*, using the low temperature single crystal refinement as an initial model.

Solid-state spectra were recorded at 96.29 (¹¹B) or 282.40 (¹⁹F) MHz using a Varian Unity Inova spectrometer and a 4 mm (rotor o.d.) magic-angle spinning probe. They were obtained using direct excitation with a 2 s (¹¹B) or 5 s (¹⁹F) recycle delay at a sample spin-rate of 10 kHz. The number of repetitions was 32 (¹¹B) and 8 (¹⁹F). Heating/cooling rates were approximately 5° per minute. Chemical shifts are referenced to an external sample of BF₃·OEt₂ or CFC₃.

Experimental Procedures for the Crystal Structure Determinations

The full diffraction datasets were collected using a Bruker X8 Apex II diffractometer, with graphite-monochromated Mo-*K*_α radiation (λ = 0.71073 Å) generated by a rotating anode. The diffractometer was fitted with an Oxford Cryostream low temperature device. The structures were solved by direct methods (*SHELXS97*^[21]), and developed by cycles of full least-squares refinement on *F*² and difference Fourier syntheses (*SHELXL97*^[21]). All crystallographic Figures were produced using *XSEED*,^[31] which incorporates *POVRAY*.^[41] Experimental data for the crystal structures are listed in Table S1.

The variable temperature unit cell data reported in the manuscript and the ESI were measured with an Agilent Supernova dual-source diffractometer, again using monochromated Mo-*K*_α radiation. The crystal was cooled or warmed between measurements at 2 Kmin⁻¹ under computer control, and poised for 10 mins at each temperature before the measurement was taken.

Crystallographic refinement of [FeL₃][BF₄]₂·*x*H₂O (**1**; *x* ≈ 3).

The same crystal was used for data collections before and after rapid cooling to 110 K, while a different crystal was used to obtain data at 300 K before, and after, slow cooling to 150 K and re-warming to room temperature. The refinement details were the same in each case. In the slow cooling experiment, cooling below 250 K resulted in twinning of the crystal which was reversed upon re-warming.

The asymmetric unit contains one-third of a complex cation and one-third of a BF₄⁻ anion, all lying on a crystallographic three-fold axis; and, a very badly disordered region, which lies within a channel running parallel to the *c*-vector of the unit cell. These channels contain another one-third equivalent BF₄⁻ ion (which is required for electroneutrality), and approximately one mole equivalent of water per asymmetric unit. A *SQUEEZE*^[51] analysis of all four datasets showed that the channels contain 61 between and 79 electrons per formula unit, with the highest value being observed for the low temperature dataset. Despite the scatter, those values agree reasonably with one BF₄⁻ and three water molecules (71 electrons in total) as predicted by elemental microanalysis.

The initial datasets, rather than the *SQUEEZED* ones, were used for the final refinements. For the slow-cooled crystal, at both temperatures the strongest Fourier peaks in the disordered region were refined as two partial BF_4^- sites, whose occupancies were refined against the average isotropic U_{eq} value of the ordered BF_4^- ion B(13)-F(15) at that that temperature. At 300 K the occupancies of these two sites refined to 0.10 and 0.09, which corresponds to 58 % of the total BF_4^- content in the disordered channels. At 110 K the same anion site occupancies refined to 0.14 and 0.12, or 78 % of the total disordered BF_4^- content. The refined restraints $\text{B-F} = 1.40(2)$ and $\text{F...F} = 2.29(2)$ Å were applied to this residue in both refinements. For the slow-cooled and rewarmed crystal, only one partial BF_4^- site could be resolved for each refinement with an occupancy of 0.10, or 30 % of the total anion content in the pores. The distance restraints in this case refined to lower values, of $\text{B-F} = 1.35(2)$ and $\text{F...F} = 2.20(2)$ Å.

The remaining contents of the asymmetric unit were not included in the final models, but are accounted for in the density and *F*000 calculations. All crystallographically ordered non-H atoms were refined anisotropically, and all H atoms were placed in calculated positions and refined using a riding model. CCDC 992761–992764.

Table S1 Experimental data for the single crystal structure determinations of **1** (C₂₁H₂₄B₂F₈FeN₁₂O₃, *M_r*, 721.99, Trigonal, space group *P31c*, *Z* = 2)

	Before rapid cooling (<i>T</i> = 300 K)	After rapid cooling (<i>T</i> = 110 K)	Before slow cooling: (<i>T</i> = 300 K)	After slow cooling to 150 K and rewarming (<i>T</i> = 300 K)
<i>a</i> (Å)	12.6729(5)	12.6653(9)	12.6778(7)	12.660(2)
<i>c</i> (Å)	10.9338(6)	11.0258(12)	10.9308(8)	10.9359(15)
<i>V</i> (Å ³)	1520.74(12)	1531.7(2)	1521.49(16)	1517.9(4)
μ (Mo-K α) (mm ⁻¹)	0.592	0.588	0.592	0.592
Measured reflections	11971	13308	21264	12294
Independent reflections	2366	1850	2090	1709
<i>R</i> _{int}	0.040	0.046	0.041	0.033
<i>R</i> ₁ [<i>I</i> > 2σ(<i>I</i>)] ^a	0.038	0.050	0.043	0.042
w <i>R</i> ₂ (all data) ^b	0.107	0.144	0.122	0.128
Goodness of fit	1.048	1.117	1.162	1.112
Flack parameter	0.010(18)	0.01(2)	0.04(2)	0.03(3)

^a*R* = $\Sigma[|F_o| - |F_c|] / \Sigma|F_o|$ ^bw*R* = $[\Sigma w(F_o^2 - F_c^2) / \Sigma wF_o^4]^{1/2}$

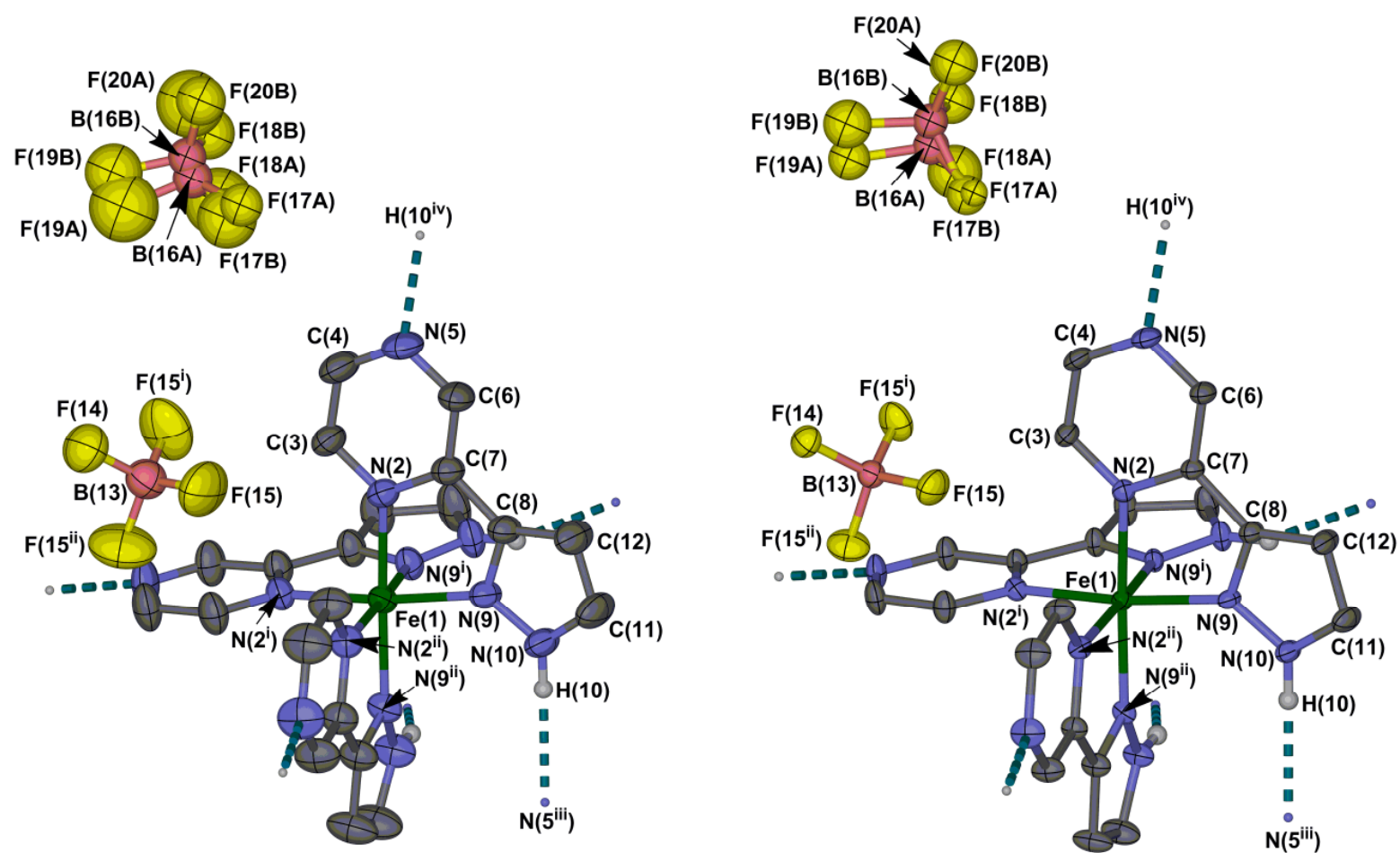


Fig S1 Contents of the asymmetric unit of **1** at 300 K (left) and 110 K (right), taken from the “rapid cooling” experiment. Displacement ellipsoids are at the 50 % probability level, and C-bound H atoms have been omitted for clarity. Colour code: C, grey; H, pale grey; B, pink; F, yellow; Fe, green; N, blue.

Atoms Fe(1), B(13) and F(14) all lie on the crystallographic C_3 axis $\frac{2}{3}, \frac{1}{3}, z$. Symmetry codes: (i) $1-y, x-y, z$; (ii) $1-x+y, 1-x, z$; (iii) $1+x-y, 1-y, -\frac{1}{2}+z$; (iv) $x-y, 1-y, \frac{1}{2}+z$.

Table S2 Selected interatomic distances and angles in the crystal structures of **1** (Å, °). See Fig. S1 for the atom numbering scheme employed. Symmetry code: (i) $1-y, x-y, z$.

	Before slow cooling ($T = 300$ K)	After slow cooling ($T = 110$ K)	Before fast cooling ($T = 300$ K)	After fast cooling to 150 K and rewarming ($T = 300$ K)
Fe(1)–N(2)	1.985(2)	1.984(3)	1.988(2)	1.982(3)
Fe(1)–N(9)	1.967(2)	1.963(3)	1.967(3)	1.969(3)
N(2)–Fe(1)–N(9)	80.25(8)	80.47(11)	80.31(10)	80.26(13)
N(2)–Fe(1)–N(2 ⁱ)	94.80(7)	94.33(10)	94.67(9)	94.54(12)
N(2)–Fe(1)–N(9 ⁱ)	88.87(9)	90.11(12)	88.83(11)	89.22(14)
N(9)–Fe(1)–N(2 ⁱ)	174.09(10)	173.42(13)	174.12(12)	173.82(14)
N(9)–Fe(1)–N(9 ⁱ)	96.33(8)	95.42(10)	96.43(10)	96.25(12)

Table S3 Hydrogen bond parameters for the crystal structures in this work (Å, °). See Figs. S1 and S2 for the atom numbering schemes employed. Symmetry codes: (iii) $1+x-y, 1-y, -1/2+z$; (vii) $-1+y, x, 1/2+z$.

	D–H	H...A	D...A	D–H...A
1 , before slow cooling ($T = 300$ K)				
C(4)–H(4)...F(17A)/F(17B)	0.93	2.55/2.40	3.383(19)/3.30(3)	149.5/163.1
N(10)–H(10)...N(5 ⁱⁱⁱ)	0.86	2.02	2.826(3)	156.7
1 , after slow cooling ($T = 110$ K)				
C(4)–H(4)...F(17A)/F(17B)	0.95	2.49/2.45	3.354(14)/3.35(2)	150.8/157.7
N(10)–H(10)...N(5 ⁱⁱⁱ)	0.88	1.98	2.810(4)	156.4
1 , before fast cooling ($T = 300$ K)				
C(4)–H(4)...F(17)	0.93	2.44	3.29(2)	152.3
N(10)–H(10)...N(5 ⁱⁱⁱ)	0.86	2.02	2.824(4)	155.8
1 , after fast cooling and rewarming ($T = 300$ K)				
C(4)–H(4)...F(17)	0.93	2.45	3.31(2)	152.8
N(10)–H(10)...N(5 ⁱⁱⁱ)	0.86	2.01	2.822(5)	156.1

Table S4 Unit cell parameters for **1** from single crystal diffraction data, and from Rietveld refinement of X-ray powder diffraction data. These data are plotted in Fig. 3 of the main paper.

Single crystal				Powder			
<i>T</i> (K)	<i>a</i> (Å)	<i>c</i> (Å)	<i>V</i> (Å ³)	<i>T</i> (K)	<i>a</i> (Å)	<i>c</i> (Å)	<i>V</i> (Å ³)
290	12.6633(6)	10.9157(5)	1515.93(12)	298	12.690(2)	10.914(3)	1522.1(7)
280	12.6573(6)	10.9227(5)	1515.47(13)				
270	12.6474(6)	10.9242(5)	1513.34(12)	273	12.666(2)	10.922(3)	1517.4(7)
260	12.6405(5)	10.9349(4)	1513.13(10)				
250	12.6362(5)	10.9325(5)	1511.77(11)	248	12.660(2)	10.931(3)	1517.4(7)
240	12.6296(6)	10.9338(5)	1510.36(12)				
230	12.6288(6)	10.9380(5)	1510.76(13)				
220	12.6398(10)	10.9440(8)	1514.2(2)	223	12.655(2)	10.941(3)	1517.5(7)
210	12.6438(13)	10.9465(10)	1515.5(3)				
200	12.6446(16)	10.9477(12)	1515.9(3)	198	12.652(3)	10.958(4)	1519.0(7)
190	12.6397(18)	10.9458(13)	1514.4(4)				
180	12.647(2)	10.9492(13)	1516.8(4)				
170	12.637(2)	10.9461(15)	1513.8(5)	173	12.646(3)	10.981(5)	1520.8(7)
160	12.643(3)	10.9530(17)	1516.1(6)				
150	12.663(3)	10.9683(19)	1523.1(6)	148	12.634(4)	11.000(5)	1520.6(8)
140	12.634(4)	10.9517(19)	1513.8(7)				
130	12.630(3)	10.9584(19)	1513.9(6)				
120	12.623(3)	10.9758(18)	1516.2(6)	123	12.623(3)	11.005(5)	1518.7(7)
110	12.624(3)	10.9778(17)	1515.2(5)				
100	12.610(2)	10.9832(15)	1512.5(4)				
110	12.640(2)	10.9937(16)	1521.0(5)				
120	12.632(3)	10.9791(17)	1517.2(5)				
130	12.621(3)	10.9621(17)	1512.1(6)				
140	12.631(3)	10.9621(18)	1514.6(6)				
150	12.642(3)	10.9621(17)	1517.3(6)				
160	12.649(3)	10.9625(17)	1519.0(5)				
170	12.642(3)	10.9537(16)	1516.0(5)				
180	12.646(2)	10.9504(14)	1516.5(4)				
190	12.6410(18)	10.9451(13)	1514.7(4)				
200	12.6442(15)	10.9474(11)	1515.8(3)				
210	12.6369(13)	10.9420(10)	1513.3(3)				
220	12.6341(10)	10.9423(8)	1512.6(2)				
230	12.6298(7)	10.9386(6)	1511.08(16)				
240	12.6337(6)	10.9444(5)	1512.80(12)				
250	12.6493(6)	10.9429(5)	1516.32(12)				
260	12.6499(5)	10.9363(5)	1515.56(11)				
270	12.6448(4)	10.9290(4)	1513.34(9)				
280	12.6495(5)	10.9222(4)	1513.50(10)				
290	12.6476(5)	10.9166(4)	1512.28(10)				

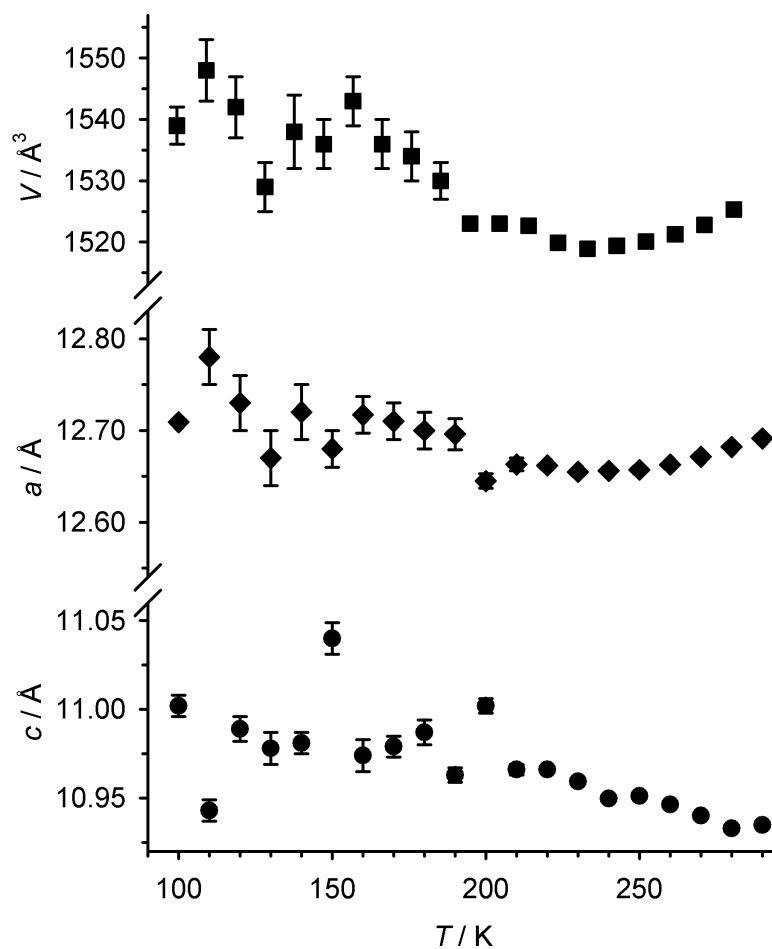


Fig S2 An alternative set of single crystal unit cell data from **1**, measured under the same conditions as the data in Fig. 3 (main article) and Table S4, but using a different crystal.

These data follow the trends in the manuscript between 300→220 K, but are too noisy at lower temperatures to interpret meaningfully. Five crystals were measured in this way during the course of this study, using two diffractometers. All the crystals showed increased errors and noise in their cell parameters below 220±20 K. The data in Fig. 3 and Table S4 also have that property, but to a lesser extent than the other crystals we examined.

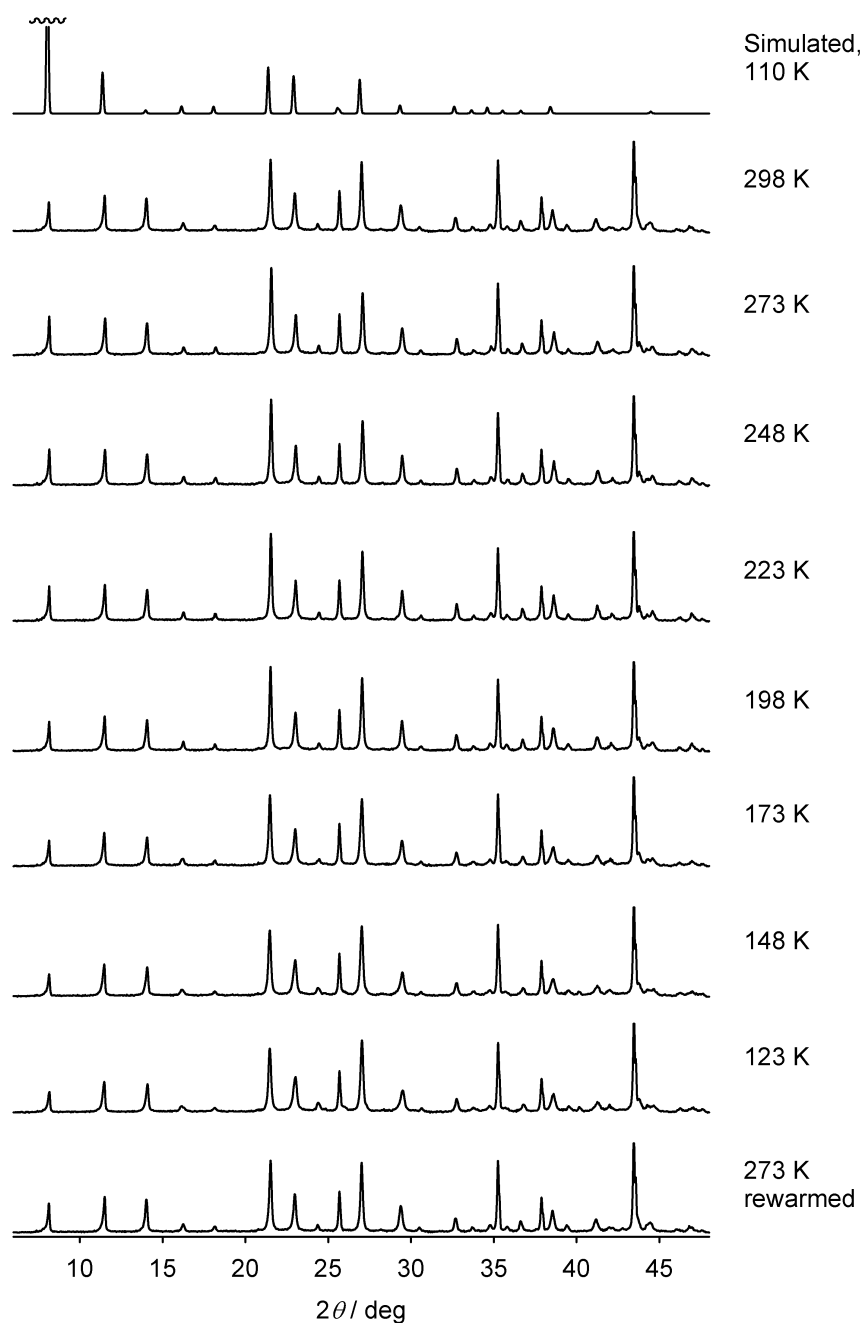


Fig S3 Observed and simulated X-ray powder diffraction data from the different phases of **1**. Data were measured in variable slit mode, and are uncorrected.

There are diffraction peaks at $2\theta = 24$ and 31° , and at $2\theta > 35^\circ$, which do not have counterparts in the simulation. These may originate from the pore contents which are not resolved in the single crystal refinements and so could not be included in the simulation.

There are no changes to the form of these powder patterns upon cooling, apart from a gradual peak broadening below 220 K which is reversed when the sample is rewarmed. This reduction in crystallinity is consistent with the increased errors on the single crystal unit cell parameters at lower temperatures (Figs. 3 and S2).

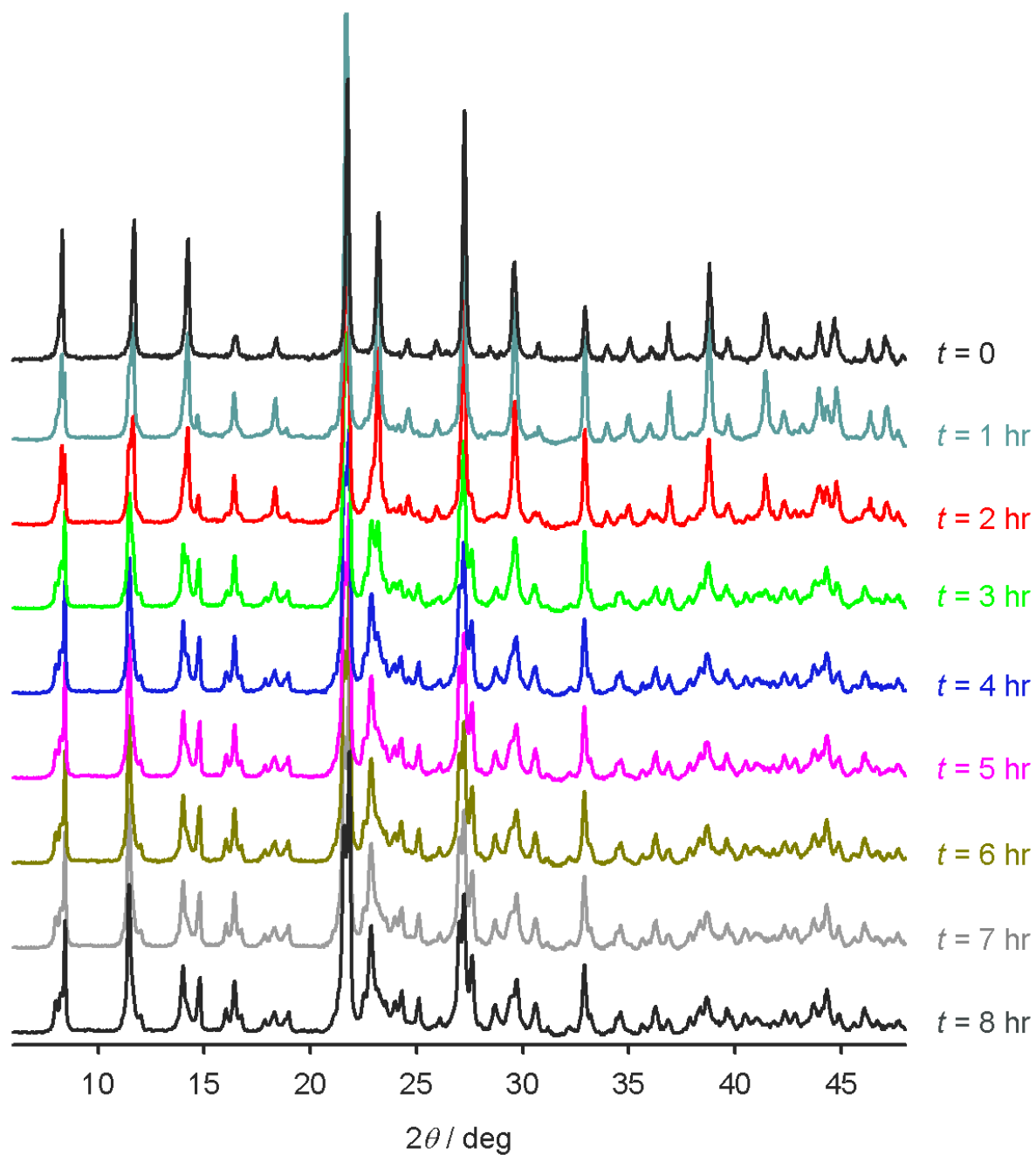


Fig S4 Changes to the X-ray powder diffraction pattern of **1** during *in situ* dehydration at 10^{-5} torr and 298 K. Data were measured in variable slit mode, and are uncorrected.

The dehydration reaction is essentially complete after 4 hrs. The dehydrated material reconverts fully to the initial phase upon exposure to air, within a period of minutes.

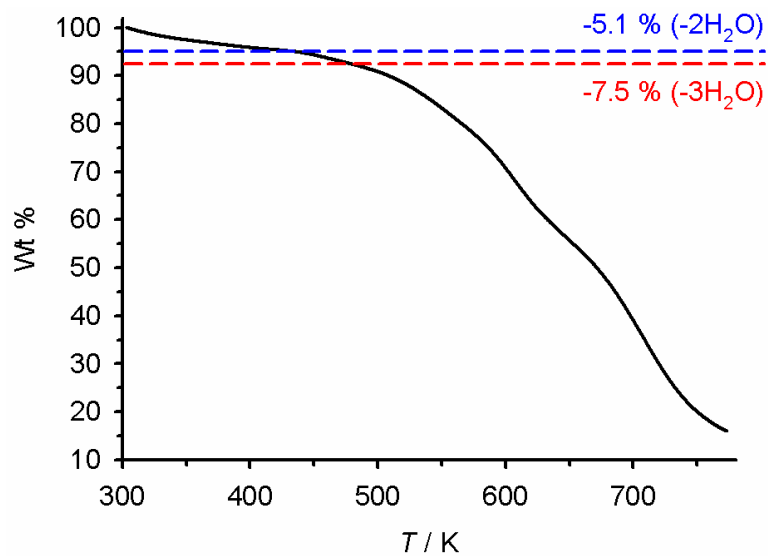


Fig S5 Thermogravimetric analysis (TGA) of **1**. The weight losses equivalent to two and three mole equivalents of water are marked.

The curve has an inflection near 440 K, at a weight loss equivalent to two mole equivalents of lattice water. The weight loss equivalent to a third mole of water occurs near 500 K, but is less well defined.

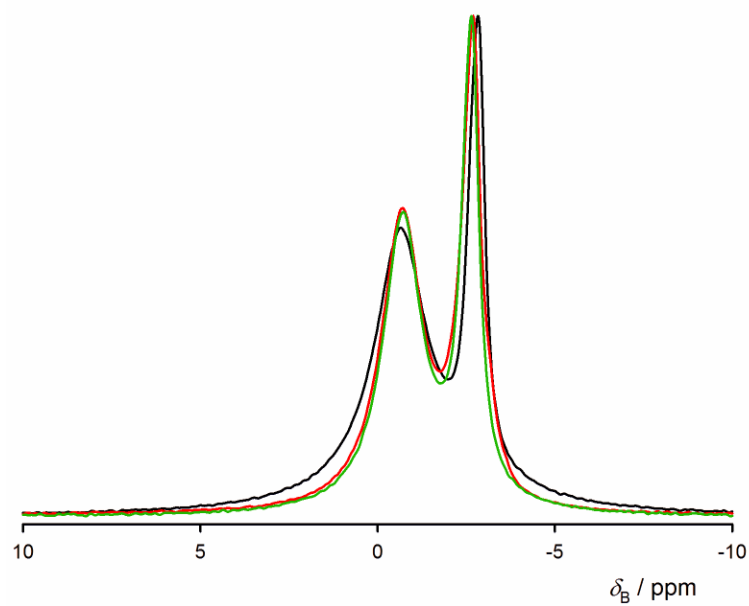


Fig S6 Solid state ^{11}B NMR spectra of **1**, at 298 (green), 238 (red) and 168 K (black).

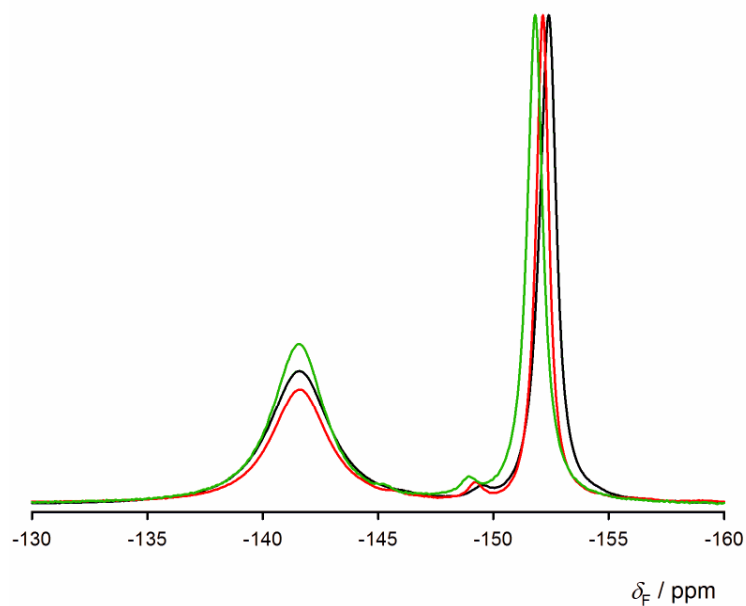


Fig S7 Solid state ^{19}F NMR spectra of **1**, at 298 (green), 238 (red) and 168 K (black).

For each nucleus we assign the broader resonance to the more static, crystallographically ordered framework BF_4^- ion; and, the narrower resonance to the (dynamically) disordered in-pore BF_4^- environment.

The weak feature at -149 ppm occurs consistently between samples, and may arise from partial hydrolysis of the in-pore BF_4^- ions to $\text{BF}_3(\text{OH})^-$.^[6]

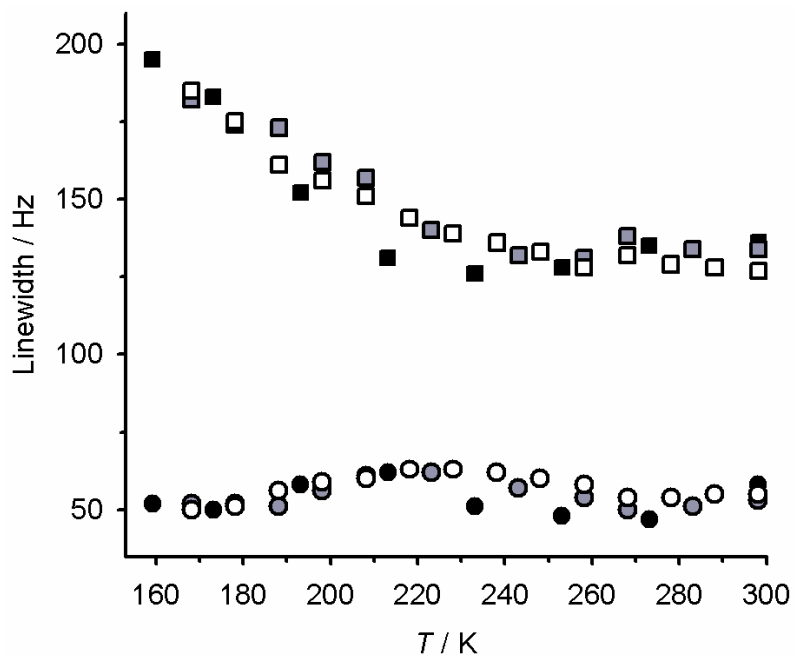


Fig. S8 ^{11}B NMR linewidths for the in-pore (circles) and framework (squares) BF_4^- ions. Data were measured using the following temperature ramps: slow cool (black); slow rewarm (grey); and rapid quench then rewarm (white).

These changes with temperature are smaller than for the ^{19}F linewidths plotted in the main article, particularly for the in-pore environment. Although the shape of the in-pore anion curve appears to follow the variable temperature unit cell dependence of **1**, the variation is barely outside the error of the experiment.

References

- [1] K. L. V. Mann, J. C. Jeffrey, J. A. McCleverty and M. D. Ward, *Polyhedron*, 1999, **18** 721.
- [2] G. M. Sheldrick, *Acta Cryst., Sect. A*, 2008, **64**, 112.
- [3] L. J. Barbour, *J. Supramol. Chem.*, 2001, **1**, 189.
- [4] *POVRAY* v. 3.5, Persistence of Vision Raytracer Pty. Ltd., Williamstown, Victoria, Australia, 2002.
- [5] A. L. Spek, *J. Appl. Cryst.*, 2003, **36**, 7.
- [6] R. J. Smithson, C. A. Kilner, A. R. Brough and M. A. Halcrow, *Polyhedron*, 2003, **22**, 725.